Modeling Temperature Distribution and Power Consumption in IT Server Enclosures with Row-Based Cooling Architectures

Hosein Moazamigoodarzi [†,1,2], *Rohit Gupta* [†,1,2], *Souvik Pal* [1], *Peiying Jennifer Tsai* [1,2], *Suvojit Ghosh* [1], *Ishwar K. Puri* [1,2*]

[1] Computing Infrastructure Research Centre, McMaster University, Hamilton, Ontario, Canada.

[2] Department of Mechanical Engineering, McMaster University, Hamilton, Ontario, Canada.

[†] HM and RG have contributed equally to the work.

AUTHOR INFORMATION

***Corresponding author**

McMaster University

1280 Main St. W.

Hamilton, ON L8S 4L7, Canada

Email: ikpuri@mcmaster.ca

Abstract

Traditional data center cooling methods cannot yet control cooling airflows and temperatures on demand, creating an intrinsic inefficiency. A recent solution places row-based cooling unit adjacent to servers and places the entire assembly within an enclosure, which improves airflow distribution and provides rapid real-time control. This is, in particular attractive for micro-data centers where traditional room-based cooling is less energy efficient. Spatiotemporal predictions of temperatures are required to control and optimize data center performance as the system configuration, and other parameters are varied. Current methods, such as proper orthogonal decomposition, machine learning, and heuristic models are inapplicable in practice because they require a prohibitively large number of *a priori* simulations or experiments to generate training datasets. We provide an alternative a computationally inexpensive training-free model for enclosed micro-data centers that are integrated with in-row cooling units that requires no *a priori* training. The model determines the air flowrate within each zone based on a mechanical resistance circuit analysis. These flowrates are then introduced into a zonal energy balance to predict the temperature of each zone. The model is validated with experimental measurements and coupled with a power consumption calculation. Its applicability is demonstrated by evaluating the influence of various system factors, such as IT server configurations, cooling unit air, and water flowrates and the numbers of cooling units, on the temperature distributions, and total cooling power consumption. The method can improve micro-data centers control and help to optimize the design of any data center with a row-based cooling system.

Key words: In-row cooling unit - Temperature prediction - Zonal method – Mechanical resistance – Energy balance – Data Center – Energy Optimization

Nomenclature

A	Surface area of heat exchanger (m^2)	V	Volume (m^3)
C_p	Specific heat capacity $\left(\frac{kJ}{kg.K}\right)$	X	Thermal mass of server $\left(\frac{kJ}{K}\right)$
P	Pressure (Pa)	ΔP	Pressure difference (Pa)
$\dot{P}_{fans}$	Power consumption of fans (W)	α	Correction factor for thermal mass
$\dot{P}_s$	Power consumption of server (W)	θ	Non-dimensional temperature
Q_c	Air flowrate through the cooling units $\left(\frac{m^3}{s}\right)$	τ	Non-dimensional time
Q_s	Air flowrate through each server $\left(\frac{m^3}{s}\right)$	ρ	Density $\left(\frac{kg}{m^3}\right)$
Q_w	Water flowrate through the cooling unit $\left(\frac{m^3}{s}\right)$	s	Server
Q_{ch}	Chiller heat load (kW)	f	Front chamber
R	Mechanical Resistance $\left(\frac{Pa.s}{m^3}\right)$	b	Back chamber
T_f	Temperature of the front chambers (K)	H	Horizontal
T_s	Temperature of server exhaust (K)	V	Vertical
T_c	Cooling unit exhaust air temperature (K)	i	Index of zone in x-direction
T_h	Cooling unit return air temperature (K)	j	Index of zone in y-direction
$T_{i,w}$	Inlet water temperature to cooling unit (K)	br	Brush
$T_{o,w}$	Outlet water temperature of cooling unit (K)	a	air
T_{ci}	Air temperature entering condenser (K)	w	water
T_{co}	Water temperature leaving evaporator (K)	ref	reference
U	Overall heat transfer coefficient $\left(\frac{W}{m^2.K}\right)$	0	Initial

1. Introduction

Increasing electricity costs have necessitated strategies to reduce the power consumed by data centers (DCs), a third of which is used to cool its IT equipment (ITE) [1, 2]. Traditional DCs typically employ air cooling, rather than direct liquid cooling, because of reliability, and lower capital and maintenance costs [3, 4]. The cold air required for the ITE is provided by cooling units that are usually placed along the server room perimeter, an architecture that is inefficient because of two significant air distribution inefficiencies, hot air recirculation and cold air bypass [5–7], which increase the cold airflow to the ITE up to two times over the required amount [8].

To address this inefficiency, an enclosed row-based cooling architecture that supplies cold air in close proximity to ITE is an alternative [9, 10]. This architecture decreases the energy required for cooling as well as the initial cost and improves agility, system availability, serviceability, and manageability. Cooling energy is reduced since airflow paths are shortened, which in turn requires less fan power and also facilitates better airflow distribution [11]. Cooling architectures with shorter airflow paths can more rapidly regulate cooling in response to dynamic changes in the ITE load or cooling unit perturbations and thus prevent the large temperature fluctuations that can produce equipment failure [12].

For the purpose of real-time control, failure prediction, and design optimization, a rapid scheme to predict temperatures in an enclosed row-based DC is required. To reduce the magnitudes of harmful temperature fluctuations, control actions should occur over a smaller duration than the timescale of a unique DC thermal event, which for enclosed row-based DC cooling is of the order of seconds [13–15]. While different methods to predicts temperatures within DC environments have been developed, such as proper orthogonal decomposition (POD), machine learning (ML), and, more recently, heuristic models, their limitations preclude implementation in operational DCs.

Compared to a full field granular physics-based model, ML and POD based data-driven models are attractive due to their quicker runtimes when coupled with control algorithms [16–19]. These data-driven models can correlate the temperature field inside a DC with operational parameters, but completely neglect the physics of the flow [20–24]. Other gray box models that capture some features of the flow, but these also have drawbacks. First, these models are auxiliary and can require an impractically large number ($\sim 10^2$-10^3) of datasets for training and accuracy. The sources for these datasets can be either real-time DC experiments, which are impractical or 3-dimensional full-field CFD simulations that are computationally expensive. Besides, to predict and control scenarios that lie outside the cluster of a training dataset, the models must extrapolate, which often leads to large errors in temperature predictions.

Other methods employ heuristic approaches that use empirical parameters to simplify the governing physical laws and then predict temperatures at the specific locations, such as server inlets [25–28]. For instance, a three-dimensional zonal model for room-based cooling with a raised floor employs a characteristic dimension of 1m to predict temperature distributions within zones in front of server racks [25]. It is intuitive that such a large zone should lead to a loss of granularity and therefore diminish the predictive accuracy. Besides, the model requires information about mass flowrates, which must be obtained from computationally expensive CFD simulations. A rapid CFD and lumped capacitance hybrid model can predict temperature fluctuations in front of servers as a function of transient events, such as server shutdown and cooling failure [26]. However, this method also requires CFD simulations for each case to determine parameters and index values. Thus, obtaining real-time temperature distributions and integrating them with the IT infrastructure control system is unfeasible with these heuristic methods.

Because it can predict temperatures with a higher resolution and accuracy than lumped models, zonal modeling is widely used for HVAC and building energy management [25, 29–33]. This method partitions a space into coarse zones assumed to have uniform physical characteristics, e.g., temperature, pressure, and velocity, to which mass and energy conservation relations are applied. The method reduces the solution time considerably by replacing the partial differential equations for mass, momentum, and energy conservation with a system of ordinary differential equations.

We developed a new parameter-free zonal transient model that is based on an analysis of mechanical resistances. The model predicted real-time temperature distributions within ITE enclosures. As a representative case study to demonstrate its applicability, an enclosed micro-DC containing separated cold and hot chambers, which is cooled by one or more in-row cooling units, was considered. The model conserved energy in each zone within the enclosure and determined its temperature. The air flowrates required to maintain energy conservation within the enclosed geometry for the pressure-driven flow were determined through an auxiliary mechanical resistance network and by applying mass conservation for each zone. This approach avoided the necessity of performing CFD simulations, experiments, or the training of empirical parameters through ML.

The novelty of the work, therefore, is the development of a computationally inexpensive mechanical resistance network approach that resolves the flow field, unlike the conventional ML or CFD based approaches available in the literature. We integrate the mechanical resistance-based flow modeling with the energy balance equations to rapidly predict the temperature distribution inside enclosed DCs for different operating conditions. The model can be employed for, (a) thermal-aware workload management, (b) development of a model-predictive controller for the

cooling units, (c) design optimization purposes, (d) investigating *what if scenarios* in DCs, and (e) fault prediction purposes.

Our objectives are to (1) demonstrate the applicability of mechanical resistance-based zonal modeling for enclosed micro-DCs that are integrated with in-row cooling units that have separated hot and front chambers, (2) validate the model using experiments, (3) investigate the effect of passive server placement on the evolution of local hot spots, (4) investigate the influence of in-row cooling unit operational parameters on the temperature distribution, (5) investigate the effect of IT load distribution across the racks and servers on chiller coefficient of performance (COP), and (6) compare thermal performance of the row-based cooling architecture when one or else two in-row cooling units are placed within the enclosure.

2. Methodology

2.1. System configuration

The geometry of an enclosed micro-DC cooled by in-row cooling units is shown in Figure 1, where the fans inside the cooling units are two prime airflow movers besides the fans in the servers. The cooling units draw warm air from a back chamber, extract heat from it and release cold air into a front chamber. The servers breathe in cold air from the front chamber and release warm air to the back chamber. The flowrate mismatch between the servers and the cooling units and the separation between the chambers creates a pressure difference $\Delta P = P_b - P_f$ between the chambers. This difference produces leakage between the chambers in the direction of the pressure differential, either from the front to the back chamber ($\Delta P < 0$) or vice versa ($\Delta P > 0$). By solving the energy balance for each zone considering the mass transfer between the two, the corresponding temperature can be determined. As mentioned, we use a mechanical resistance network to determine the flowrates within the enclosure instead of performing CFD simulations.

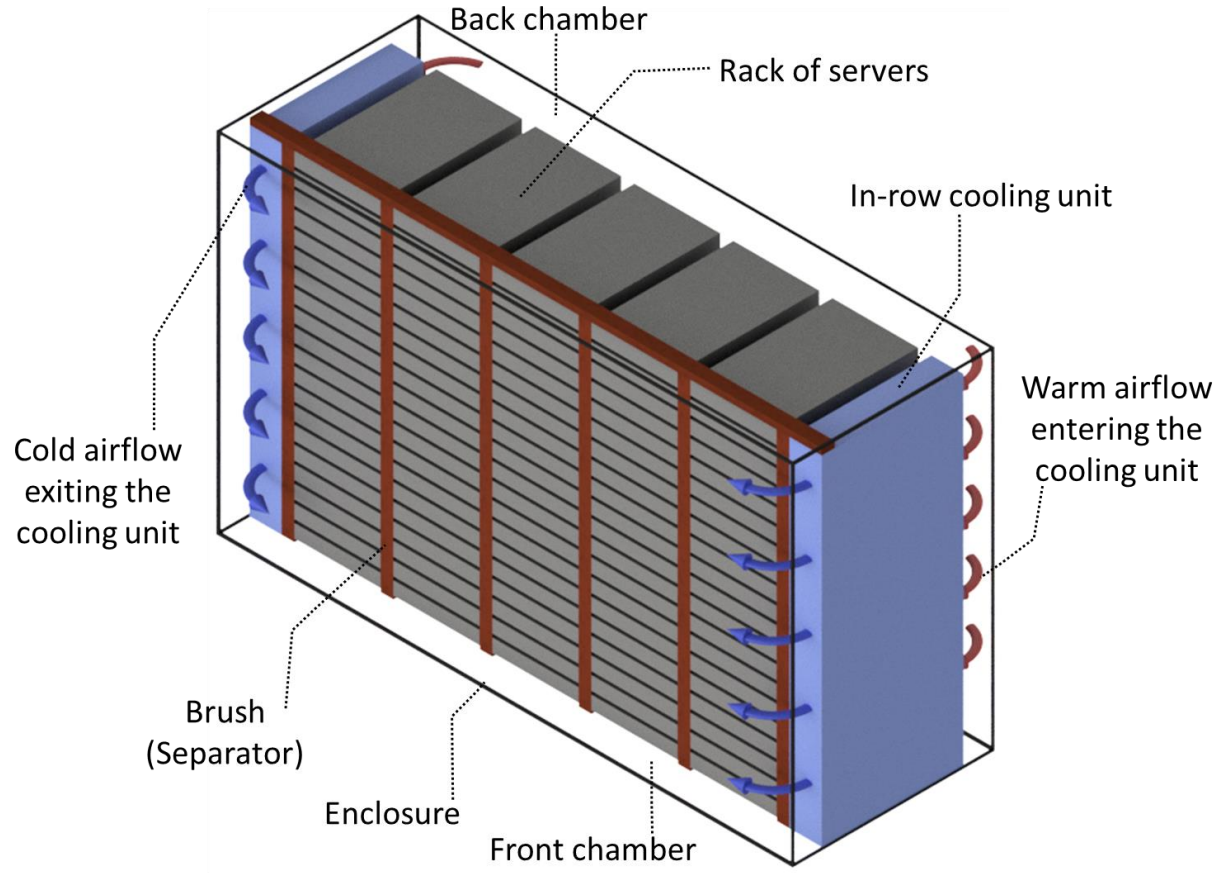

Figure 1: Schematic of the IT enclosure integrated with five IT racks and two in-row cooling units (CUs) with separated cold and back chambers. In the front chamber, cold air is delivered by the CUs and is drawn into the servers. In the back chamber, hot air exits the servers and is drawn into the CUs. There is leakage airflow through the brushes that separate the two chambers, either from the hot to the front chamber or vice versa depending upon the pressure differences.

The zones inside the enclosure are presented in Figure 2. Neglecting heat and mass transfer between the enclosure and its ambient, six control volumes are considered, i.e., (1) the zones in front of each server, (2) the zones at the back of each server, (3) the zones in front of the cooling units, (4) the zones at the back of the cooling units, (5) each server itself, and (6) the cooling unit. The cooling unit contains a heat exchanger that transfers heat from the warmed air to a chilled water loop that is supplied by an external system consisting of a chiller and circulation pump.

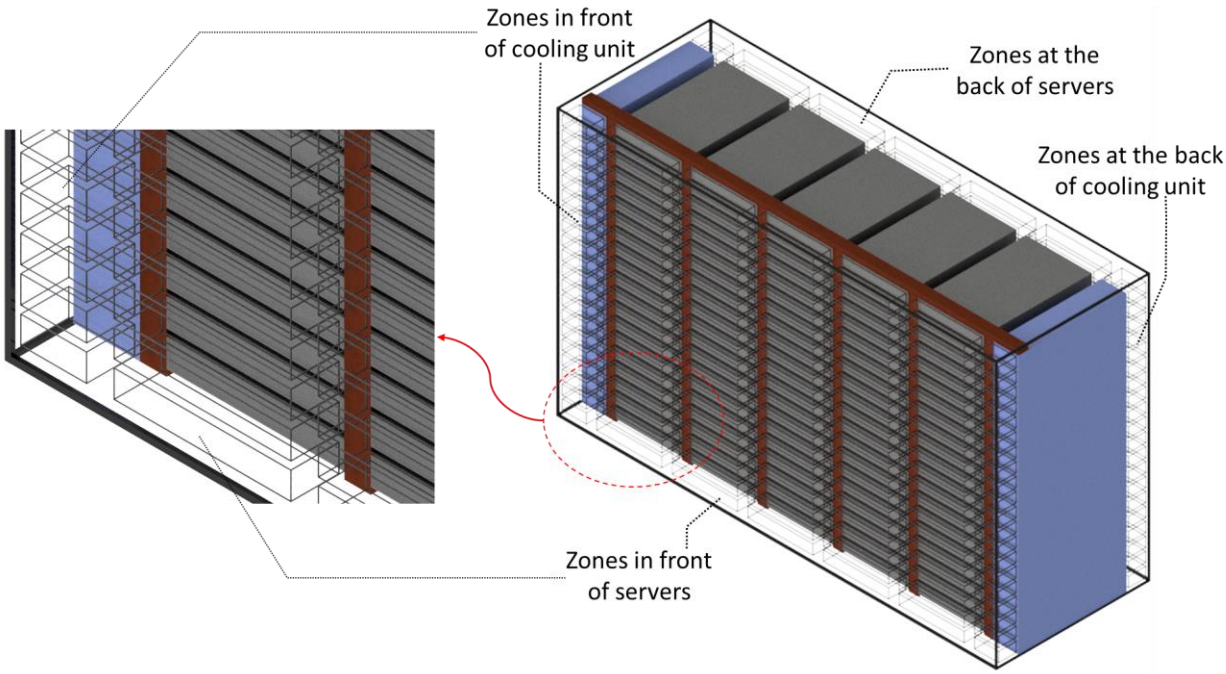

Figure 2: Zones considered inside the enclosure.

2.2. Flow-resistance network representation and flowrate calculation

Enclosed DCs contain a pressure driven airflow for which mechanical resistances can be described to determine the flowrates. The mechanical resistance network for the system is depicted in Figure 3, where voltage is analogous to pressure and current to airflow. The in-row cooling units are thus represented as a source of current, or the air flowrates Q_c. Each active server is a single current source since it draws in specific air flowrate Q_s. A passive server, i.e., one that is not powered, is a resistance R_s that is a porous separator which allows air to travel across the back and front chambers. Essentially, a passive server behaves as a porous duct through which the flowrate responds to the pressure difference between the front and back chambers [34]. Separators (or brushes) create resistances, R_{br} that prevent air leakage between the front and back chambers. The resistances to airflows along the vertical heights of the front and back chambers are denoted as $R_{f,V}$ and $R_{b,V}$, respectively, and those along the horizontal widths of the front and back chambers are likewise $R_{f,H}$ and $R_{b,H}$.

The flow Q_c is an order of magnitude larger than Q_s. Although $R_{br} > R_s$, these two resistances are of the same order of magnitude, but $R_{f,H}, R_{f,V}, R_{b,H}$, and $R_{b,V}$ are all an order of magnitude smaller in comparison because the characteristic dimensions of the corresponding chambers are an order of magnitude larger than those of the holes in the brushes and server channels through which air flows.

If the flowrate from the cooling units is smaller than the total flowrate through the servers, the resulting pressure difference ΔP is positive, i.e., hot air leaks through the passive servers and brushes into the front chamber. On the other hand, if the flowrate from the cooling units is larger than the total flowrate through the servers, ΔP is negative, i.e., cold air now leaks from the front into the back chamber.

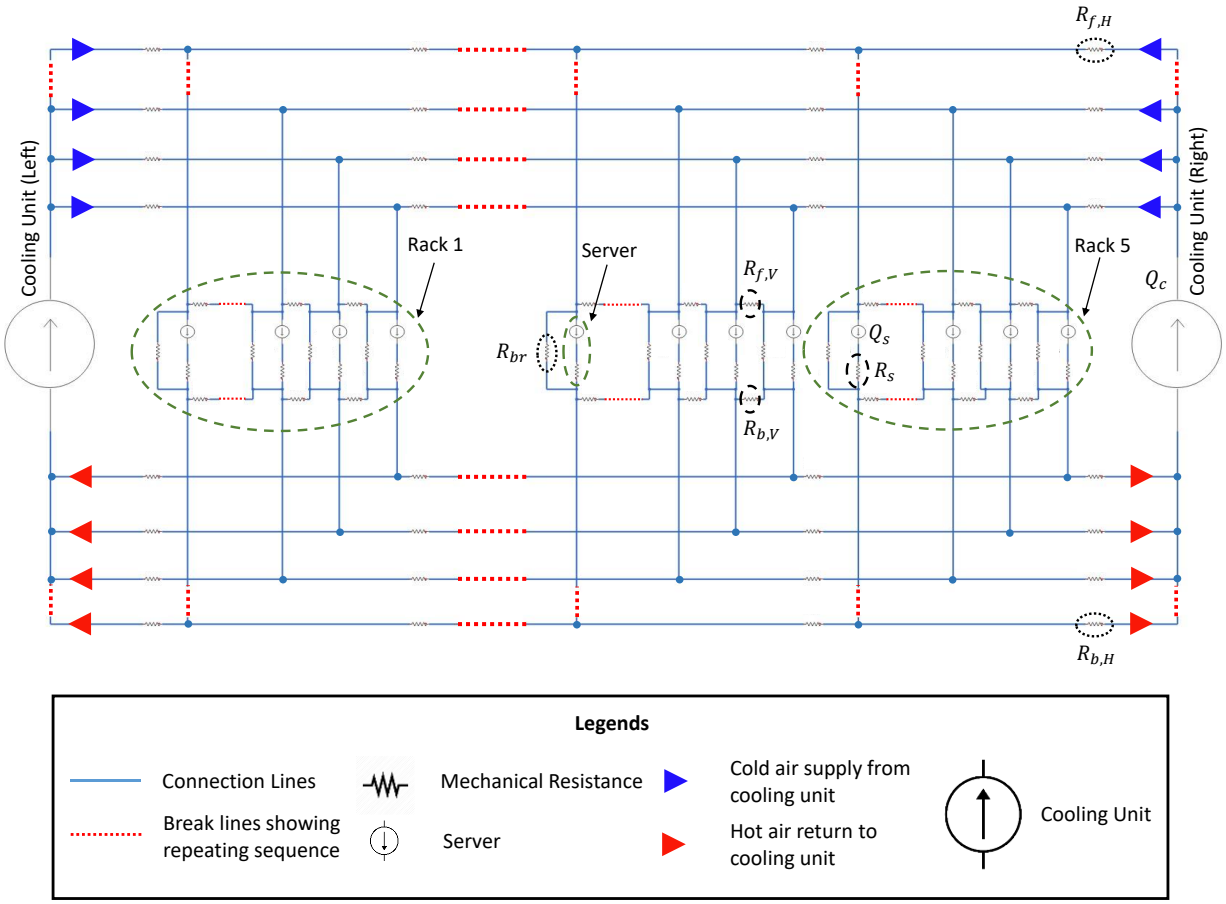

Figure 3: Generalized flow resistance network inside the IT server enclosure with five racks (each having 20 servers) and two in-row cooling units. The red and blue arrows show the warm air return and cold air supply path from the cooling unit. The repeating sequences of servers and mechanical resistances are shown with red dotted line.

The air flowrate through the cooling units is determined by the fan control system so that the flow through the in-row cooling unit is solely a function of its fan speed. However, the flowrate of the air drawn by each active server is a function of the server fan speed and the pressure difference between the front and the back of that server. The pressure difference between the chambers is typically of the order of 10 Pa [34], which is not significant enough to influence the flowrate. Consequently, airflow through a server is essentially a function of its fan speed alone. We can therefore assume that the airflow through each active server equals the measured airflow in open space. Since the inlet air temperature is the only factor influencing server fan speed, the air flowrate through an active server is a function of the temperature of the zone in front it. For sake of example, the airflow through an HP ProLiant DL360 G5 server is [34],

$$Q_{s,i,j} = \begin{cases} 0.01415 & if \quad T_{i,j,f} < 25°C \\ 0.01415 + \left(T_{i,j,f} - 25\right) \times 0.00142 & if \quad 25°C < T_{i,j,f} < 35°C \end{cases}. \tag{1}$$

In Figure 4, the zone in front of each server interacts with six airflows, i.e., the air exchange is between a zone of interest and the zones that (1) lie below it, i.e., $Q_{j\to j-1}$ and (2) lie above it, $Q_{j\to j+1}$, and on its (3) left, $Q_{i\to i-1}$ and (4) right, $Q_{i\to i+1}$, (5) within the corresponding server $Q_{i,j,s}$, and (6) the leakage airflow from the front to the back chamber $Q_{i,j,l}$. A mass balance conducted for the zones in front of active servers reveals,

$$\begin{aligned} &[(P_{i+1,j,f} - P_{i,j,f})/R_{f,H}]^{m} + [(P_{i-1,j,f} - P_{i,j,f})/R_{f,H}]^{m} + [(P_{i,j+1,f} - P_{i,j,f})/R_{f,V}]^{m} \\ &+ [(P_{i,j-1,f} - P_{i,j,f})/R_{f,V}]^{m} + [(P_{i,j,b} - P_{i,j,f})/R_{br}]^{m} - Q_{i,j,s} = 0 \end{aligned} \tag{2}$$

where m characterizes the relationship between the pressure drop and the flowrate, P denotes pressure, i and j are the horizontal and vertical indices of the zones, respectively, and f represents the zones in front of the servers.

With the mass balance for the zones in front of passive servers,

$$[(P_{i+1,j,f} - P_{i,j,f})/R_{f,H}]^{m} + [(P_{i-1,j,f} - P_{i,j,f})/R_{f,H}]^{m} + [(P_{i,j+1,f} - P_{i,j,f})/R_{f,V}]^{m} + [(P_{i,j-1,f} - P_{i,j,f})/R_{f,V}]^{m} + [(P_{i,j,b} - P_{i,j,f})/R_{br}]^{m} + + [(P_{i,j,b} - P_{i,j,f})/R_{s}]^{m} = 0, \quad (3)$$

Considering the mass balance for the zones at the back of active servers,

$$[(P_{i+1,j,b} - P_{i,j,b})/R_{b,H}]^{m} + [(P_{i-1,j,b} - P_{i,j,b})/R_{b,H}]^{m} + [(P_{i,j+1,b} - P_{i,j,b})/R_{b,V}]^{m} + [(P_{i,j-1,b} - P_{i,j,b})/R_{b,V}]^{m} + [(P_{i,j,f} - P_{i,j,b})/R_{br}]^{m} + Q_{s,i,j} = 0, \quad (4)$$

where b represents the zones at the back of the servers.

The mass balance for the zones at the back of passive servers reveals,

$$[(P_{i+1,j,b} - P_{i,j,b})/R_{b,H}]^{m} + [(P_{i-1,j,b} - P_{i,j,b})/R_{b,H}]^{m} + [(P_{i,j+1,b} - P_{i,j,b})/R_{b,V}]^{m} + [(P_{i,j-1,b} - P_{i,j,b})/R_{b,V}]^{m} + [(P_{i,j,f} - P_{i,j,b})/R_{br}]^{m} + [(P_{i,j,f} - P_{i,j,b})/R_{s}]^{m} = 0, \quad (5)$$

The mass balance for the zones in front of the cooling unit leads to,

$$\sum_{j} [(P_{i+1,j,f} - P_{i,j,f})/R_{f,H}]^{m} = Q_{c}, \quad (6)$$

where Q_c denotes the cooling unit volumetric air flowrate. Similarly, the mass balance for the zones at the back of the cooling unit is,

$$\sum_{j} [(P_{i+1,j,b} - P_{i,j,b})/R_{b,H}]^{m} = Q_{c}, \quad (7)$$

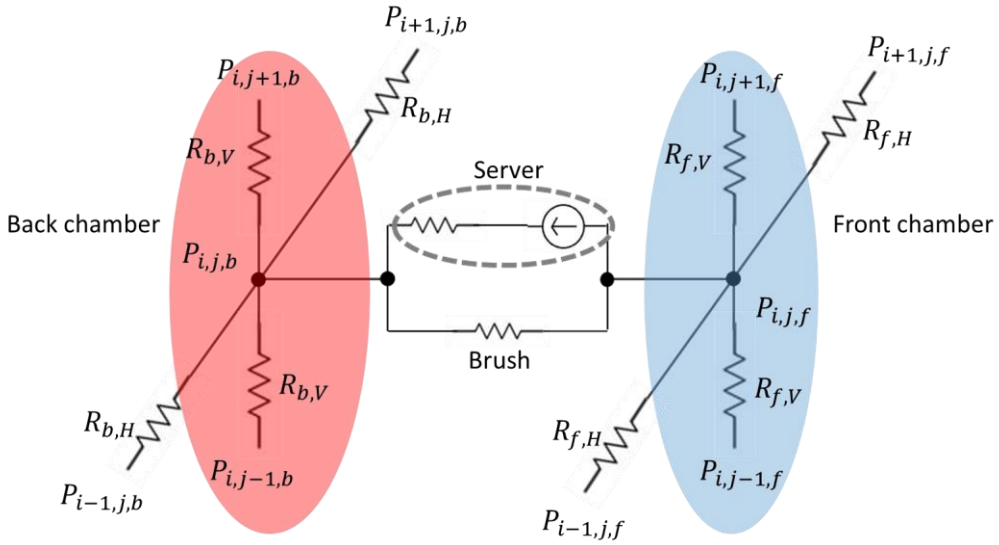

Figure 4: Airflows in the zones in front (right) and at the back (left) of servers.

To solve Eq. (1) - (7) and calculate the corresponding air flowrates for all zones we require the values of m and the resistances. The resistances of the front and back chambers are determined through experiments on an enclosed modular DC that contains two in-row cooling units with separated chambers, as shown in Figure 1. To measure the total pressure difference, a differential pressure sensor is used. The volumetric flowrate is calculated by measuring the average air velocity and the cross-section area. The average velocity is calculated by measuring the air velocity at five different points within each sectional area using a Testo-405 anemometer. The pressure drop with respect to the volumetric flowrate for the front and back chambers is reported in Figure 5.

The mechanical resistances of the passive servers and brushes are also determined experimentally by measuring the pressure drops and the air flowrates through them. The air flowrate is measured by a Kanomax TABmaster™ 6710 Flow Capture Hood with 0.00235 m^3/s accuracy and a differential pressure sensor is used to measure the pressure drop. The variation of pressure drop with respect to volumetric flowrate for the passive servers and brushes is presented in Figure 6a and 6b respectively. Based on Figures 5 and 6, $m \approx 1$ for all resistances so that these

resistances can be reasonably extracted from both figures. We note that a different value, e.g., $m = 0.5$ denoting a parabolic relation between pressure drop and air flowrate can also be applied [35]. Applying equations (1) - (7) for all servers and their corresponding zones, results in a system of linear equations that provide the pressure for each zone.

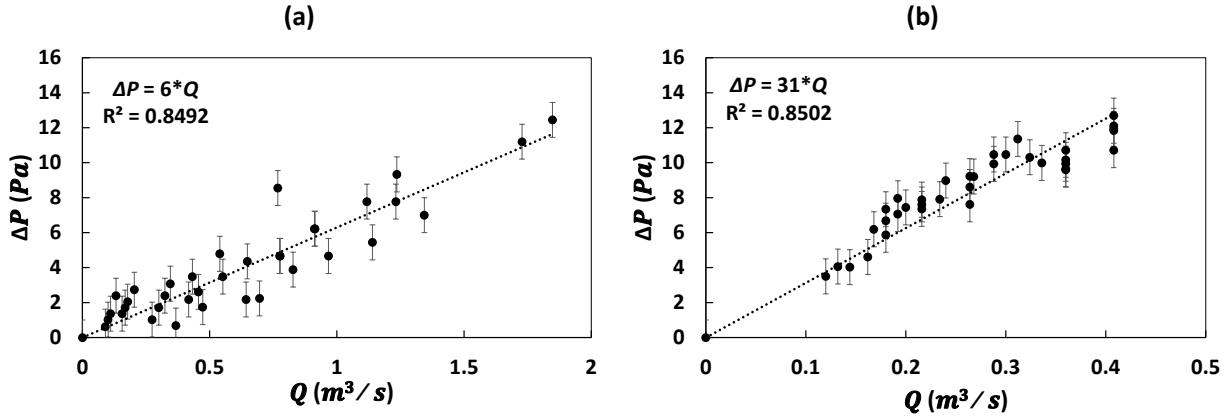

Figure 5: Pressure drop *vs*. volumetric air flowrate for the (a) cold front and (b) warm back chambers.

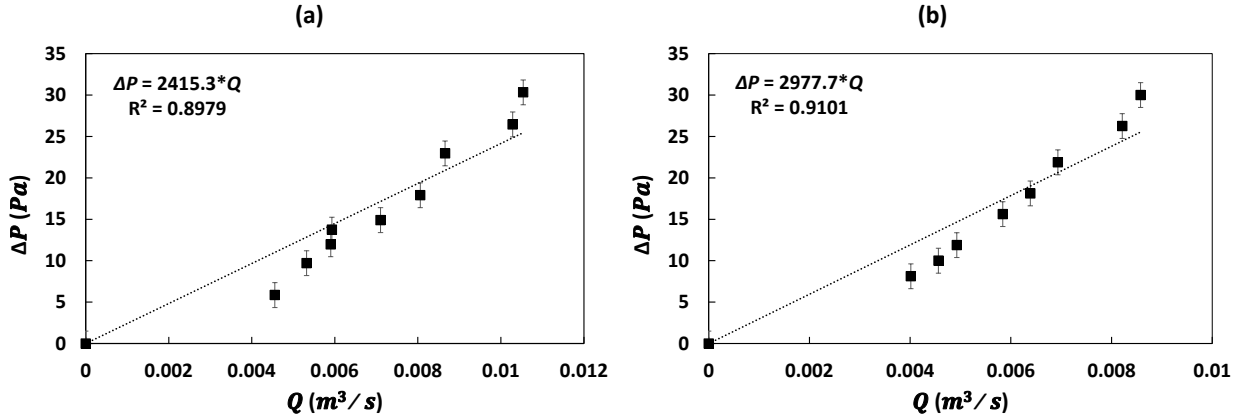

Figure 6: Pressure drop *vs.* volumetric air flowrate for (a) passive servers and (b) brushes.

2.3.Formulation of energy balance equations

Once the pressure of a zone and the mechanical resistances across it are known, the entering and exiting air flowrates through it can be calculated and the energy balances obtained thereupon. The energy balance for an active server is,

$$\frac{X}{2}\left(\frac{dT_{i,j,s}}{dt}+\frac{dT_{i,j,f}}{dt}\right)=\rho_a c_{p,a} Q_{i,j,s}\left(T_{i,j,f}-T_{i,j,s}\right)+\dot{P}_{i,j,s}, \tag{8}$$

where $T_{i,j,s}$ denotes the server exhaust temperature, $T_{i,j,f}$ the temperature of the zone in front of the server, ρ_a air density, $c_{p,a}$ the specific heat of air, X the thermal mass of the server that is available in the literature [36], and $\dot{P}_{i,j,s}$ the total power consumption of the corresponding server. For the airside of the in-row cooling unit,

$$\rho_a c_{p,a} V_a\left(\frac{dT_c}{dt}+\frac{dT_h}{dt}\right)=\rho_a c_{p,a} Q_c(T_h-T_c)-\frac{UA}{2}\left(T_h+T_c-T_{i,w}-T_{o,w}\right), \tag{9}$$

and for the waterside within that unit,

$$\rho_w c_{p,w} V_w\left(\frac{dT_{i,w}}{dt}+\frac{dT_{o,w}}{dt}\right)=\rho_w Q_w c_{p,w}\left(T_{i,w}-T_{o,w}\right)+\frac{UA}{2}\left(T_h+T_c-T_{i,w}-T_{o,w}\right), \tag{10}$$

where T_c denotes the air temperature at the exhaust of the in-row cooling unit, T_h the temperature of air entering the cooling unit, $T_{i,w}$ and $T_{o,w}$ the chilled water inlet and warm water outlet temperatures, Q_w the water flowrate, $c_{p,w}$ the specific heat of water, ρ_w the density of water, U the overall heat transfer coefficient inside the in-row cooling unit, which is a function of Q_c and Q_w, A the contact area on each fluid side, and V_a and V_w the air and water volumes inside the heat exchanger. Since the value of UA for air to water heat exchanger is a weak function of the water flowrate that depends primarily on the air flowrate, it is a function of Q_c.

For the zones in front and back of servers, the energy balance is,

$$\rho_a c_{p,a} V_z \alpha\left(\frac{dT_{i,j}}{dt}\right)=\phi_1+\phi_2+\phi_3+\phi_4+\phi_5+\phi_6, \tag{11}$$

where α is a correction factor for the thermal masses of the zones which is experimentally determined, V_z the volume of the chamber, and ϕ the energy exchange for the zones. Table 1 contains expressions for each term in Equation (11).

Table 1: Expressions for the terms in Equation 11.

Zones in front of the servers		Zones at the back of the servers	
ϕ_1		ϕ_1	
$(P_{i+1,j,f} - P_{i,j,f}) \geq 0$	$\rho_a c_{p,a} [(P_{i+1,j,f} - P_{i,j,f})/R_{f,H}] \; T_{i+1,j,f}$	$(P_{i+1,j,b} - P_{i,j,b}) \geq 0$	$\rho_a c_{p,a} [(P_{i+1,j,b} - P_{i,j,b})/R_{b,H}] \; T_{i+1,j,b}$
$(P_{i+1,j,f} - P_{i,j,f}) < 0$	$\rho_a c_{p,a} [(P_{i+1,j,f} - P_{i,j,f})/R_{f,H}] \; T_{i,j,f}$	$(P_{i+1,j,b} - P_{i,j,b}) < 0$	$\rho_a c_{p,a} [(P_{i+1,j,b} - P_{i,j,b})/R_{b,H}] \; T_{i,j,b}$
ϕ_2		ϕ_2	
$(P_{i-1,j,f} - P_{i,j,f}) \geq 0$	$\rho_a c_{p,a} [(P_{i-1,j,f} - P_{i,j,f})/R_{f,H}] \; T_{i-1,j,f}$	$(P_{i-1,j,b} - P_{i,j,b}) \geq 0$	$\rho_a c_{p,a} [(P_{i-1,j,b} - P_{i,j,b})/R_{b,H}] \; T_{i-1,j,b}$
$(P_{i-1,j,f} - P_{i,j,f}) < 0$	$\rho_a c_{p,a} [(P_{i-1,j,f} - P_{i,j,f})/R_{f,H}] \; T_{i,j,f}$	$(P_{i-1,j,b} - P_{i,j,b}) < 0$	$\rho_a c_{p,a} [(P_{i-1,j,b} - P_{i,j,b})/R_{b,H}] \; T_{i,j,b}$
ϕ_3		ϕ_3	
$(P_{i,j+1,f} - P_{i,j,f}) \geq 0$	$\rho_a c_{p,a} [(P_{i,j+1,f} - P_{i,j,f})/R_{f,V}] \; T_{j+1,j,f}$	$(P_{i,j+1,b} - P_{i,j,b}) \geq 0$	$\rho_a c_{p,a} [(P_{i,j+1,b} - P_{i,j,b})/R_{b,V}] \; T_{i,j+1,b}$
$(P_{i,j+1,f} - P_{i,j,f}) < 0$	$\rho_a c_{p,a} [(P_{i,j+1,f} - P_{i,j,f})/R_{f,V}] \; T_{i,j,f}$	$(P_{i,j+1,b} - P_{i,j,b}) < 0$	$\rho_a c_{p,a} [(P_{i,j+1,b} - P_{i,j,b})/R_{b,V}] \; T_{i,j,b}$
ϕ_4		ϕ_4	
$(P_{i,j-1,f} - P_{i,j,f}) \geq 0$	$\rho_a c_{p,a} [(P_{i,j-1,f} - P_{i,j,f})/R_{f,V}] \; T_{j-1,j,f}$	$(P_{i,j-1,b} - P_{i,j,b}) \geq 0$	$\rho_a c_{p,a} [(P_{i,j-1,b} - P_{i,j,b})/R_{b,V}] \; T_{i,j-1,b}$
$(P_{i,j-1,f} - P_{i,j,f}) < 0$	$\rho_a c_{p,a} [(P_{i,j-1,f} - P_{i,j,f})/R_{f,V}] \; T_{i,j,f}$	$(P_{i,j-1,b} - P_{i,j,b}) < 0$	$\rho_a c_{p,a} [(P_{i,j-1,b} - P_{i,j,b})/R_{b,V}] \; T_{i,j,b}$
ϕ_5		ϕ_5	
$(P_{i,j,b} - P_{i,j,f}) \geq 0$	$\rho_a c_{p,a} [(P_{i,j,b} - P_{i,j,f})/R_{br}] \; T_{i,j,b}$	$(P_{i,j,f} - P_{i,j,b}) \geq 0$	$\rho_a c_{p,a} [(P_{i,j,f} - P_{i,j,b})/R_{br}] \; T_{i,j,f}$
$(P_{i,j,b} - P_{i,j,f}) < 0$	$\rho_a c_{p,a} [(P_{i,j,b} - P_{i,j,f})/R_{br}] \; T_{i,j,f}$	$(P_{i,j,f} - P_{i,j,b}) < 0$	$\rho_a c_{p,a} [(P_{i,j,f} - P_{i,j,b})/R_{br}] \; T_{i,j,b}$
ϕ_6 (for passive server)		ϕ_6 (for passive server)	
$(P_{i,j,b} - P_{i,j,f}) \geq 0$	$\rho_a c_{p,a} [(P_{i,j,b} - P_{i,j,f})/R_s] \; T_{i,j,b}$	$(P_{i,j,f} - P_{i,j,b}) \geq 0$	$\rho_a c_{p,a} [(P_{i,j,f} - P_{i,j,b})/R_s] \; T_{i,j,f}$
$(P_{i,j,b} - P_{i,j,f}) < 0$	$\rho_a c_{p,a} [(P_{i,j,b} - P_{i,j,f})/R_s] \; T_{i,j,f}$	$(P_{i,j,f} - P_{i,j,b}) < 0$	$\rho_a c_{p,a} [(P_{i,j,f} - P_{i,j,b})/R_s] \; T_{i,j,b}$
ϕ_6 (for Active server)		ϕ_6 (for Active server)	
$-\rho_a c_{p,a} Q_{i,j,s} T_{i,j,f}$		$\rho_a c_{p,a} Q_{i,j,s} T_{i,j,s}$	

The dimensionless forms of temperature and time are,

$$\theta = \frac{T - T_{ref}}{T_0 - T_{ref}}, \qquad (a) \qquad\qquad \tau = \frac{t}{t_0}, \qquad (b) \qquad (12)$$

where T_{ref} and t_0 denote reference values for temperature and time and T_0 the initial temperature. Hence, the dimensionless forms of the energy equations for the server are

$$\frac{d\theta_{i,j,s}}{d\tau} + \frac{d\theta_{i,j,f}}{d\tau} = \frac{2\rho_a c_{p,a} Q_{i,j,s} t_0}{X}\left(\theta_{i,j,f} - \theta_{i,j,s}\right) + \frac{2t_0 \dot{P}_{i,j,s}}{X(T_0 - T_{ref})}, \tag{13}$$

and for the in-row cooling units,

Airside:
$$\frac{d\theta_c}{d\tau} + \frac{d\theta_h}{d\tau} = \frac{2Q_c t_0}{V_a}(\theta_h - \theta_c) - \frac{2t_0 UA}{\rho_a c_{p,a} V_a}\left(\theta_h + \theta_c - \theta_{i,w} - \theta_{o,w}\right), \tag{14}$$

Waterside:
$$\frac{d\theta_{i,w}}{d\tau} + \frac{d\theta_{o,w}}{d\tau} = \frac{2Q_w t_0}{V_w}\left(\theta_{i,w} - \theta_{o,w}\right) + \frac{2t_0 UA}{\rho_w c_{p,w} V_w}\left(\theta_h + \theta_c - \theta_{i,w} - \theta_{o,w}\right). \tag{15}$$

For zones in the front and back of the servers, the dimensionless form of the relation is,

$$\frac{d\theta_{i,j}}{d\tau} = \sum_{k=1}^{6} \frac{\Phi_k t_0}{\rho_a c_{p,a} V_z \alpha (T_0 - T_{ref})}, \tag{16}$$

The procedure to determine the temperature of each zone at a particular time follows,

- Step 1: Specify the initial temperatures.
- Step 2 : Prescribe Q_c and Q_w.
- Step 3 : Determine the flowrates by applying equations (1) - (7) for all zones and solve the system of linear equations.
- Step 4 : Solve equations (13) - (16) for all zones to determine the temperatures at a particular time
- Step 5 : repeat the process by advancing it by $\Delta\tau$.

Since all differential equations are of first order and linear, Euler's method is employed to solve them numerically using MATLAB R2018a.

2.4. Power consumption calculation

The temperature distribution alone is insufficient to characterize the influence of different system parameters. Hence, the power consumption of the cooling components must also be determined. For the present configuration, the primary energy consuming components include (1) in-row cooling unit blowers, (2) chilled water pumps. and (3) the chiller. The chilled water pumps consume at most 3% of total cooling power [36], such that for a 30% increase in water pumping power, which is in any case unlikely to occur, the total cooling power change is a negligible 1%. Hence, only components (1) and (3) are considered. To determine the energy consumption of in-row cooling unit blowers and the chiller, the total heat rejection from ITEs, total cooling unit air flowrate, chilled water temperature entering the in-row cooling unit, and the ambient air temperature must be known.

The power consumed by the refrigeration system in the chiller is a function of (1) the heat load of its evaporator Q_{ch}, (2) the temperature of ambient air entering condenser T_{ci}, (3) the desired setpoint temperature of the chilled water leaving the evaporator T_{co}, and (4) other operating and design parameters, including the loading of the chiller with respect to its rated capacity (COP). While there are several analytical models available in the literature that characterize chiller operation, the Gordon–Ng model is selected for its simplicity and ease since readily available data can fit model coefficients. The model has the form [37],

$$y = a_1 x_1 + a_2 x_2 + a_3 x_3, \text{ where} \tag{17}$$

$$x_1 = T_{co}/Q_{ch}, \tag{18}$$

$$x_2 = (T_{ci} - T_{co})/(T_{ci} \times Q_{ch}), \tag{19}$$

$$x_3 = ([(1/COP) + 1] \times Q_{ch})/T_{ci}, \text{ and} \tag{20}$$

$$y = [(1/COP) + 1] \times (T_{co}/T_{ci}) - 1, \quad (21)$$

where COP denotes the coefficient of performance defined as the ratio of the evaporator heat load to the electrical power consumed by the compressor, T_{ci} the temperature of ambient air entering condenser, T_{co} the chilled water temperatures leaving the chiller, respectively, and Q_{ch} the chiller heat load. Based on this model, the power consumption for each specific chiller is not a function of refrigerant temperature. In our case, the T_{co} i.e. the chilled water temperature is equal to the $T_{i,w}$ i.e. the water temperature delivered to the in-row cooling units. Data for Q_{ch}, COP, T_{ci}, and T_{co} are obtained from the manufacturer of a 50 kW chiller [38] that, when fitted to Equation (17), provide the relation,

$$y = 0.023x_1 + 1.39x_2 + 0.32x_3. \quad (22)$$

Since the condenser temperature is assumed constant, we use 9 data points at a constant condenser temperature for regression for which the residual sum of squares is 1.4×10^{-6}. Equation (22) provides the chiller power consumption once the total cooling load, evaporator temperature, and condenser temperature are known.

The power consumption of the fans inside the in-row cooling unit is calculated for the Rittal TopTherm-LCP-Rack-CW [39]. Based on its data sheet and its fan [40], the relation between the air flowrate provided and the power consumption is,

$$\dot{P}_{fans} = 480 - 3073Q_c + 6031Q_c^2 \quad (23)$$

where $\dot{P}_{fans}$ denotes the total power consumption of the fans inside each cooling unit.

3. Results and discussion

3.1. Model validation

To validate the model, the temperature profiles for an arbitrary IT load distribution are experimentally measured for three different cooling unit air flowrates and compared with model predictions. The experiments are performed on an enclosed modular DC with separated chambers. The DC has five racks and two in-row cooling units located at the ends. The conditions of racks and cooling units during validation experiments are presented in Table 2.

Table 2: Operating conditions of racks and cooling units for the validation experiments

Rack	IT load (kW)	Airflow rate (m^3/s)
1	3.82	0.18
2	3.57	0.17
3	4.04	0.2
4	3.94	0.17
5	3.72	0.18

Scenario	Cooling Unit	Setpoint (°C)	Airflow rate (m^3/s)
High	Left	18	0.65
($Q_c > \sum Q_s$)	Right	18	0.65
Medium	Left	18	0.45
($Q_c \sim \sum Q_s$)	Right	18	0.45
Low	Left	18	0.35
($Q_c < \sum Q_s$)	Right	18	0.35

Figure 7 demonstrates this comparison for three cooling unit air flowrates, i.e., (a) high ($Q_c > \sum Q_s$), (b) medium ($Q_c \sim \sum Q_s$), and (c) low ($Q_c < \sum Q_s$). The total IT load of the racks is 20kW. Each rack contains 5 temperature sensors, i.e., 25 sensors are mounted at different locations in the front chamber. The percentage of relative error (ε) with respect to the measured temperatures at each location is defined as,

$$\varepsilon = \frac{T_f^{exp} - T_f^{model}}{T_f^{exp}} \times 100 \quad (24)$$

Figure 7.a shows that the relative percentage error between the model and the experiment is lower than 3%. The probability of hot spot formation is low due to cold air oversupply which results in more a uniform temperature distribution in the front chamber. In Figure 7.b, the relative error between the model and experiment for 20 locations is lower than 5%, for 4 locations smaller than 7.5%, and for a single location it is 10% . In Figure 7.c, for 20 locations the deviation of the predictions from measurements is again lower than 5%, for 3 locations it is smaller than 7.5%, and for two locations it is 9%. For the last two cases, more hot spots appear in the cooler front chamber because the cold air flowrate is lower. Overall though, Figure 7 shows that the model predicts the temperature distribution reasonably well.

a

0.6	1.1	-1.6	-0.5	-0.6
0.6	-0.6	-1.1	0.6	2.3
-2.2	-0.6	-1.1	-1.1	1.1
-1.1	-0.6	-1.6	-0.6	0.6
0.6	-1.1	-1.6	-1.6	-0.5

$Q_c > \sum Q_s$

b

-2.7	4.0	-2.8	-3.6	-1.1
-1.7	0.0	4.2	-1.1	-1.1
-2.8	2.2	4.7	0.5	-1.1
-4.0	0.0	-4.2	5.8	2.8
-6.5	-7.4	-9.7	1.0	5.9

$Q_c \sim \sum Q_s$

c

3.1	0.3	-0.6	-5.6	1.6
2.2	1.8	0.8	1.9	-0.5
4.3	-0.9	-3.8	-1.0	0.0
5.4	-4.1	0.8	-2.7	-4.5
7.4	7.4	-0.9	-9.3	-8.5

$Q_c < \sum Q_s$

Figure 7: Percentage error (ε) between the temperature predicted by the model and the measured temperature at 25 different locations in the front chamber. (a) High cooling unit air flowrate, i.e., $Q_c > \sum Q_s$. (b) Medium cooling unit air flowrate, i.e., $Q_c \sim \sum Q_s$. (c) Low cooling unit air flowrate, i.e., $Q_c < \sum Q_s$. The total IT load of the racks is 20 kW. Green, yellow, and red colors specify that ε is lower than 5 %, 7.5 %, and 10 % respectively.

3.2.Influence of passive server location

Passive servers that are not utilized in DCs are usually switched off. In an enclosed DC with separated hot and front chambers, passive servers act as porous ducts connecting the two chambers. This behavior enables flow and energy transport across the chambers and significantly influences the temperature of the front chamber. We investigate when (a) a passive server plays an important

role in altering the front chamber temperature, and (b) the influence of its location inside the enclosure. The simulation conditions are presented in Table 3.

Table 3: Operating conditions of racks and cooling units for the simulation scenarios in Figure 8.

Rack	IT load (kW)	Number of passive servers
1	4.5	5
2	4.5	5
3	4.5	5
4	4.5	5
5	4.5	5

Scenario	Cooling Unit	Water Inlet Temperature (°C)	Airflow rate (m^3/s)
High	Left	12	0.68
($Q_c > \sum Q_s$)	Right	12	0.68
Medium	Left	12	0.50
($Q_c \sim \sum Q_s$)	Right	12	0.50
Low	Left	12	0.4
($Q_c < \sum Q_s$)	Right	12	0.4

Figure 8 demonstrates the influence of cooling unit air flowrate on the temperature distribution in the front chamber in presence of passive servers for the micro-DC configuration of Figure 1. Each rack is assumed to contain five passive servers. For all the scenarios, we consider the same water flowrate and water inlet temperature.

Based on Figure 8, when the cooling unit air flowrate is high, or $Q_c > \sum Q_s$, a passive server does not have any effect on the temperature distribution. When the cooling unit air flowrate $Q_c \leq \sum Q_s$, the hot air recirculation through the passive server increases. As shown in Figure 3, passive servers are mechanical resistances and the direction of the airflow through them is a function of pressure difference across the servers. If the air flowrate of the cooling units is greater than that drawn by the servers, or $Q_c > \sum Q_s$, the pressure of the front chamber is higher than that of the back chamber, resulting in air flow through the passive servers from the front to the back

chamber, a phenomena known as cold air bypass. If the air flowrate of the cooling units is lower than that drawn by the servers, i.e., $Q_c \leq \sum Q_s$, the pressure in the front chamber is lower than in the back chamber, resulting in air flow through the passive server from the back to the front chamber, termed as hot air recirculation.

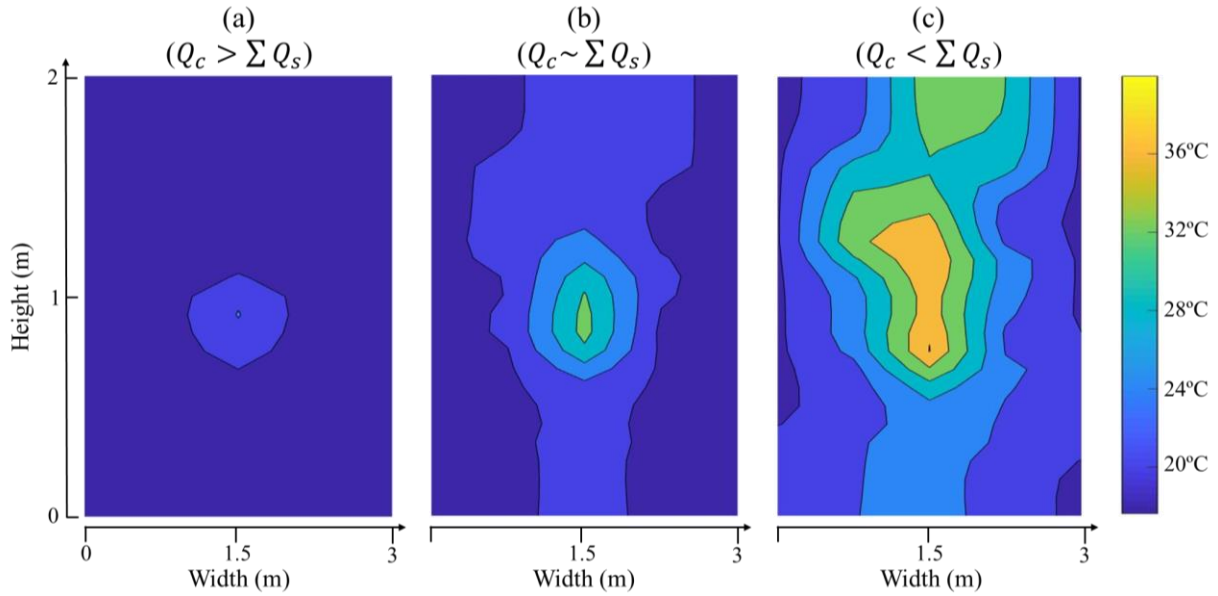

Figure 8: Influence of cooling unit air flowrate on the temperature distribution of the front chamber in the presence of passive servers.

The location of a passive server, specifically its distance from the cooling unit, influences the airflow distribution and consequently the temperature distribution, since the mechanical resistance circuit depends on the location of the passive server. The simulation conditions for studying the influence of passive server location are presented in Table 4.

Table 4: Operating conditions of racks and cooling units for the simulation scenarios in Figure 9.

Case a			**Case b**			**Case c**		
Rack	IT load (kW)	Number of passive servers	Rack	IT load (kW)	Number of passive servers	Rack	IT load (kW)	Number of passive servers
1	0	20	1	4.5	0	1	4.5	0
2	4.5	0	2	0	20	2	4.5	0
3	4.5	0	3	4.5	0	3	0	20
4	4.5	0	4	4.5	0	4	4.5	0
5	4.5	0	5	4.5	0	5	4.5	0
Cooling Unit			Water Inlet Temperature (°C)			Airflow rate (m^3/s)		
Left			12			0.50		
Right			12			0.50		

Figure 9 presents the influence of passive server location on the maximum and average temperatures in the front chamber. For all cases, the air and water flowrates, and water inlet temperature of the cooling unit are the same. Each case considers 20 passive servers within a rack of interest.

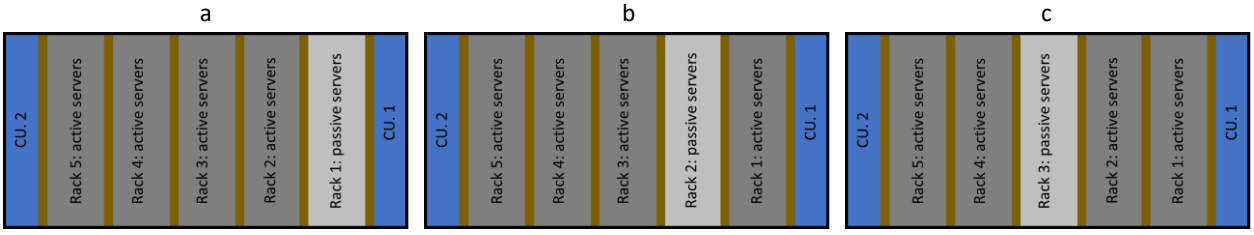

Case	Average temperature of the front chamber (°C)	Maximum temperature of the front chamber (°C)
a	20.8	25.2
b	21.7	29.3
c	23.5	37.5

Figure 9: Influence of passive server location on the maximum and average temperature in the front chamber.

It is evident from Figure 9 that placing passive servers near the cooling units reduces the magnitude of hot air recirculation through these servers. The recirculation through passive servers

is a function of the pressure difference ($P_b - P_f$) across them. Moving from the cooling unit toward the middle of the rack, P_f decreases and P_b increases, increasing ($P_b - P_f$) which in turn increases the hot air recirculation through passive servers. Thus, passive servers should be placed in proximity to the in-row cooling unit to minimize hot air recirculation.

3.3. Effect of water inlet temperature, water flowrate, and air flowrates of the cooling unit

In this section we investigate the influence of the (1) water inlet temperature, (2) water flowrate, and (3) air flowrate of the cooling unit on the temperature distribution in the front chamber and the cooling power consumption for an arbitrary load distribution. The simulation conditions are presented in Table 5.

Table 5: Operating conditions of racks and cooling units for the simulation scenario in Figure 10.

Rack	IT load (kW)	Number of passive servers
1	4.5	5
2	4.5	5
3	4.5	5
4	4.5	5
5	4.5	5

Case	Cooling units water flowrate (m^3/s)	Cooling units water Inlet Temperature (°C)	Cooling units air flowrate (m^3/s)	Cooling units power consumption (kW)
1.a	0.00051	11.25	0.57	6.76
1.b	0.00051	12.5	0.57	6.59
1.c	0.00051	13.75	0.57	6.42
2.a	0.00045	13	0.55	6.36
2.b	0.00051	13	0.55	6.36
2.c	0.00056	13	0.55	6.36
3.a	0.00051	13	0.495	6.01
3.b	0.00051	13	0.55	6.36
3.c	0.00051	13	0.605	6.79

Figure 10 depicts the influence of a 10% change in each of these three parameters (corresponds to the nine scenarios in table 5). Figure 10.1 shows that a 1.25 °C reduction in water inlet temperature results in 1.3 °C rise in the average temperature of the front chamber, whereas the cooling power changes by only 170 W, an overall 2.5% increase. Figure 10.2 reveals that a 10% change in the water flowrate does not significantly influence the temperature distribution, but a 10% change in the air flowrate (Figure 10.3) alters the average front chamber temperature by 3.1 °C. Although changing the water flowrate does not alter the cooling power consumption since water flow is regulated by controlling the valves, increasing the air flowrate by 10% results in a 430 W increment, or a 7% change, in cooling power consumption.

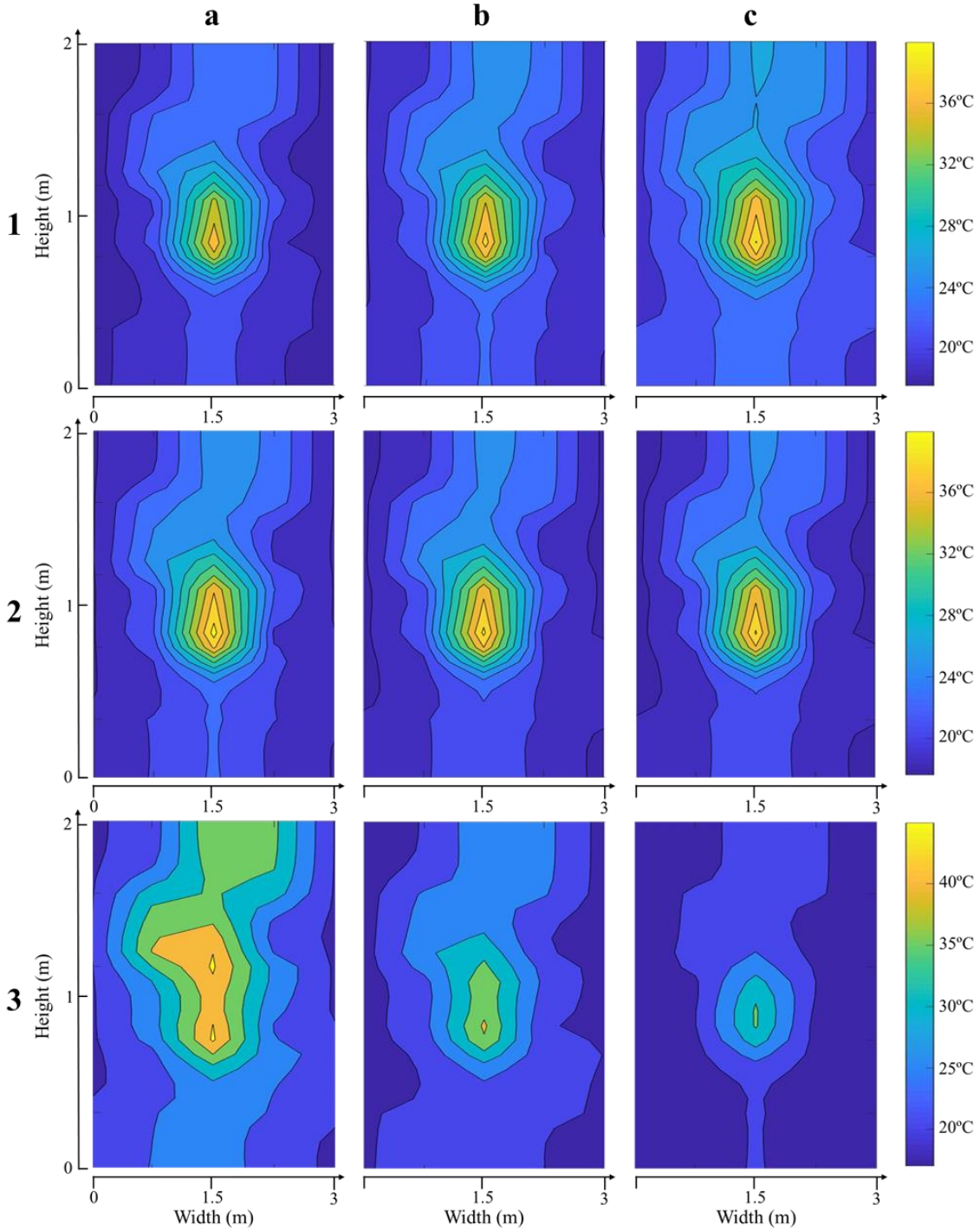

Figure 10: (1) Influence of water inlet temperature, (2) water flowrate, and (3) air flowrate of the in-row cooling unit on temperature distribution and power consumption.

The cooling unit employs an air to water finned tube heat exchanger for which,

$$T_{air} = (Q/R_{tot-HE}) + T_{water} \quad (25)$$

where R_{tot-HE} denotes the total thermal resistance of the heat exchanger, T_{air} and T_{water} the average temperatures of the air and water inside the heat exchanger respectively, and Q the heat transfer rate. Increasing water flowrate results in a minor reduction in R_{tot-HE}, while increasing air flowrate considerably reduces R_{tot-HE} because the total thermal resistance of the heat exchanger includes three thermal resistances, i.e., (1) through the metallic body of the heat exchanger (which is 5% of the total), (2) metal body to water (15%), and (3) metal body to air (80%) [41]. This is supported by Figure 10 where a 10% reduction in the air flowrate produces an appreciable increase in temperature compared to a proportional change in the water flowrate.

The water inlet temperature does not influence R_{tot}, implying a linear relation (see Equation 25) between T_{water} and T_{air}, which is supported by Figure 10.1. For all cases demonstrated in Figure 10, the heat load at steady state is constant.

3.4. Effect of IT load on coefficient of performance (COP)

The cooling system efficiency is measured by calculating the COP as the ratio of total heat load (the IT load in this case) to the cooling power consumption. We investigate the effect of IT load on the COP for our specific DC architecture. Figure 11 describes the relationship between the IT load and COP. Figure 11.a shows that increasing the IT load by changing the utilization improves the cooling efficiency because (1) the total air flowrate drawn by the servers remains constant, and (2) the temperature of heat source, i.e., CPU temperature, increases, resulting in a larger temperature difference between the hottest (CPU junction) and coldest (chilled water) points of the system, in turn improving the heat transfer efficiency. Figure 11.b shows that increasing the IT

load by changing the number of servers reduces the cooling efficiency because the total air flowrate drawn by the servers increases, resulting in higher fan power consumption in the cooling unit. Therefore, to increase cooling energy efficiency, the IT load should be increased by increasing utilization but not the number of active servers.

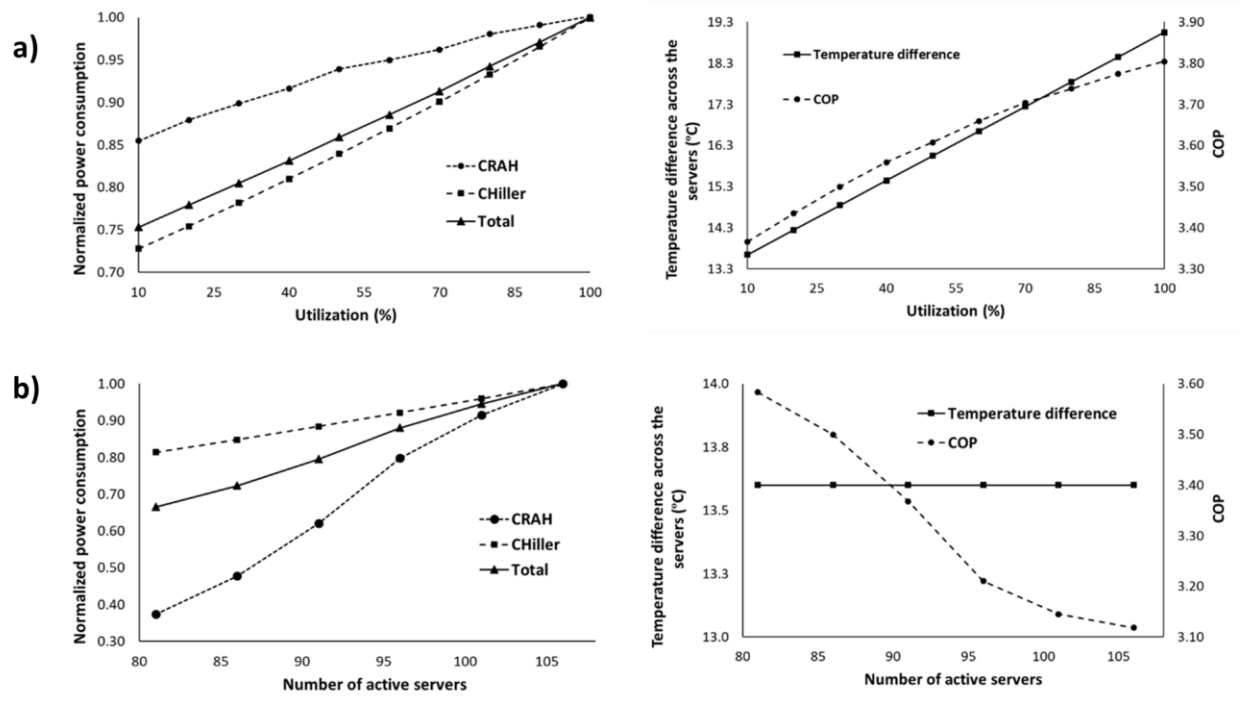

Figure 11: Effect of IT load on the on the cooling power consumption (left), temperature difference across the servers and COP (right). (a) The number of servers is constant, and the IT load is increased by increasing the utilization of each server. (b) The utilization of each server remains constant, but the IT load is increased by increasing the number of active servers.

3.5. Comparing a single in-row cooling unit with two in-row cooling units

The above cases consider two in-row cooling units within the enclosure that are located at the left and right ends of the rows. Table 6 compares cooling of an enclosed row with two in-row cooling units and a single unit, keeping the IT load distribution, geometry and other parameters for both cases the same. The air flowrates into the cooling units are adjusted to maintain a maximum temperature no greater than 27ºC in the front chamber. Installing two cooling units results in a lower average temperature in the front chamber as well as lower power consumption. Farther away

from the cooling unit, the pressure in the front chamber is reduced while the pressure in the back chamber increases (Figure 3), i.e., $(P_b - P_f)$ and the intensity of hot air recirculation through the passive server increase. For a single cooling unit, the rack farthest from the cooling unit is now the fifth rack. The temperature distribution is more uniform with two cooling units, leading to a lower required cold air flowrate and lower fan power consumption. The reason for lower power consumption for scenario (b) in Table 6 is that the relation between air flowrate and power consumption is parabolic. Thereby, distributing the total required air flowrate to a larger number of fans considerably reduces the total power consumption.

Table 6: Comparison of the cooling performance for an enclosed row with a single in-row cooling unit and one with two in-row cooling units.

Parameters	**(a) One cooling unit**	**(b) Two cooling units**
Maximum temperature of the front chamber (℃)	27	27
Average temperature of the front chamber (℃)	21.4	18.2
Total air flowrate of the cooling units (m^3/s)	1.49 (1.49 + 0)	1.35 (0.675 + 0.675)
Fan power consumption (kW)	4.2	2.1
Chiller power consumption (kW)	5.3	5.3
Total cooling power consumption (kW)	9.5	7.4
IT load (kW)	24	24

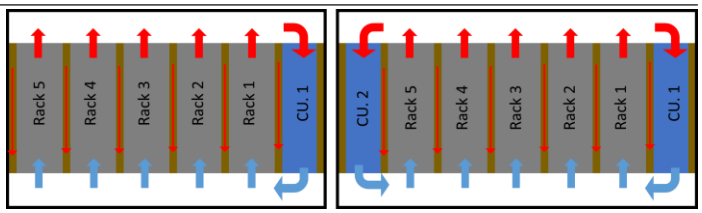

3.6. Comparison with other temperature prediction tools

Temperature prediction tools inform the controllers and facilitate failure prognosis. Hence, the computational time required to accurately predict the temperature distribution is an important

consideration. Compared to CFD, the model described here is able to more quickly determine temperatures. The model provides results in less than 60s, while a CFD simulation for a similar geometry takes hours [17, 21, 34]. For instance, if a DC design requires that a hundred cases be investigated, the model can provide results in less than 100 minutes whereas it would take around 4 days to perform the corresponding CFD simulations. This time-saving advantage of the model makes it suitable for real-time control. ML-based temperature prediction tools, which use experimental data, usually require about 15 hours of training for a specific geometry and IT load distribution [42, 43]. Some ML-based tools which use CFD simulations as their source require even a longer duration. For example, a model reported in the literature that requires CFD simulations takes 28 hours to run on a computer equipped with a Quadcore Intel i7 CPU @ 3.4 GHz and 8 GB of RAM [20]. Another model requires 30 different CFD simulations for training to predict the temperature in front of 30 servers [21]. We use an Intel (R) Core (TM) i7 6700 HQ CPU @ 2.6 GHz with 16 GB of RAM. Since the model solves the energy balance for each zone at each time step, the computational time increases linearly when the numbers of zones and the prediction times increase. The time interval to advance the simulation for all cases is 0.001 seconds. Increasing this interval to 0.01 seconds decreases the computational time by a tenth. Table 7 compares the method with other temperature prediction methods reported in the literature.

Table 7: Comparison of the method with other available temperature prediction tools for data centers.

	Assessment Criteria	CFD [6, 11, 20, 24-26]	Data-driven methods* (ANN, SVR, GPR and POD) [16-24, 44]	Lumped system approach [25-28]	Present work
1	Required time to simulate one specific scenario	Hours/days	Minutes	Seconds	Minutes
2	Required time to train, calibrate, or setup the model	Hours/days	Hours/days	Minutes	Hour
3	Resolution	O (mm)	O (m)	O (m)	O (cm)
4	Whether redoing the training is required upon changing, • Servers • Cooling configuration • IT loads	Yes	Yes	No	No
5	Captures spatial and temporal variations in temperature	Yes	Yes	Only temporal	Yes
6	Extrapolation accuracy	NA	Depends on the method (Poor for SVR and GPR)	NA	NA
7	Interpolation accuracy	NA	Good	NA	NA
8	Captures airflow leakages through gaps and passive servers	Yes	No	No	Yes
9	Number of datasets required for training/calibration	NA	~10^2-10^3	NA	NA
10	Whether the model can be integrated with a control system	No	Yes	Yes	Yes

*ANN: Artificial Neural Network, SVR: Support Vector Regression, GPR: Gaussian Process Regression, POD: Proper Orthogonal Decomposition.

4. Conclusion

We demonstrated an efficient model to characterize the real-time temperature distribution within an IT server enclosure integrated with an in-row cooling unit. The flow field is predicted based on mechanical resistances and coupled with zonal energy balance equations, a process that is

computationally less expensive than typical methods. In contrast, to control schemes such as proper orthogonal decomposition, machine learning, and other heuristic models, the model requires no *a priori* training. Upon experimental validation, model predictions of the temperatures deviate at most by 9% relative to the experimental measurements. The model is also combined with cooling power consumption calculations to determine the influence of different IT infrastructure parameters on energy consumption for cooling.

The influence of the (1) locations of passive servers, (2) cooling unit water inlet temperature, flowrate, and air flowrates, (3) imposed IT load distribution, and (4) utilization of two cooling units rather than a single unit are investigated. Salient findings include:

1. Passive servers should be located in racks closer to the cooling unit to maintain a colder temperature in the front chamber.
2. A 10% change in water flowrate increases temperatures in the front chamber by lower than 2%. A 10% increase in the water temperature increases the average temperature in the front chamber by 7% and decreases the cooling power consumption by 2.5%.
3. Increasing the airflow rate by 10% increases the cooling power consumption by 7% and decreases the mean temperature in the front chamber by 13%.
4. To increase the cooling energy efficiency, the IT load should be increased by increasing the utilization of each server rather than increasing the number of servers.
5. Using two in-row cooling units to lower the portion of the total cooling capacity provided by each unit decreases the front chamber temperature on average by 15%. It offers up to a 22% reduction in cooling power consumption as compared to using a single in-row unit that carries the entire cooling capacity.

The proposed model can be employed for the following applications in data center cooling infrastructure,

a. Thermal-aware workload management,
b. Model-predictive controller development for the cooling units,
c. Design optimization purposes,
d. Investigating *what-if scenarios* in DCs,
e. Fault prediction and diagnosis purposes.

5. Acknowledgment

This research was supported by the Natural Sciences and Engineering Research Council (NSERC) of Canada under a collaborative research and development (CRD) project, "Adaptive Thermal Management of Data Centers". We also thank our colleagues from CINNOS Mission Critical Inc. who provided insight and expertise that assisted the research.

6. References

[1] A. Shehabi, S. Smith, D. Sartor, R. Brown, M. Herrlin, "United States Data Center Energy Usage Report, LBNL-1005775", BERKELEY NATIONAL LABORATORY, 2016.

[2] J. Dai, M. M. Ohadi, D. Das, and M. G. Pecht, "Optimum Cooling of Data Centers, Application of Risk Assessment and Mitigation Techniques", Springer Science Business Media, New York, 2014, DOI: 10.1007/978-1-4614-5602-5.

[3] K. Ebrahimi, G. F. Jones, and A. S. Fleischer, "A review of data center cooling technology, operating conditions and the corresponding low-grade waste heat recovery opportunities," Renew. Sustain. Energy Rev., vol. 31, no. Supplement C, pp. 622–638, Mar. 2014.

[4] H. M. Daraghmeh and C.-C. Wang, "A review of current status of free cooling in datacenters," *Appl. Therm. Eng.*, vol. 114, no. Supplement C, pp. 1224–1239, Mar. 2017.

[5] M. K. Patterson, "The effect of data center temperature on energy efficiency," in *2008 11th Intersociety Conference on Thermal and Thermomechanical Phenomena in Electronic Systems*, 2008, pp. 1167–1174.

[6] J. Cho, J. Yang, and W. Park, "Evaluation of air distribution system's airflow performance for cooling energy savings in high-density data centers," *Energy Build.*, vol. 68, no. PARTA, pp. 270–279, 2014.

[7] H. Moazamigoodarzi, S. Pal, D. Down, M. Esmalifalak, and I. K. Puri, "Perfoamne of A Rack Mountable Cooling Unit in an IT Server Enclosure", *Thermal Science and Engineering progress*, 2019. https://doi.org/10.1016/j.tsep.2019.100395.

[8] S. V. Patankar, "Airflow and Cooling in a Data Center," *J. Heat Transfer*, vol. 132, no. 7, p. 073001, 2010.

[9] T. Evans, "The different types of air conditioning equipment for IT environments," *APC White Pap.*, p. 24, 2004.

[10] K. Dunlap and N. Rasmussen, "Choosing Between Room, Row, and Rack-based Cooling for Data Centers," *Schneider Electr. White Pap. 130*, p. 18, 2012.

[11] H. Moazamigoodarzi, P. Jennifer, S. Pal, S. Ghosh, and I. K. Puri, "Influence of cooling architecture on data center power consumption," *Energy*, vol. 183, pp. 525–535, 2019.

[12] N. El-Sayed, I. A. Stefanovici, G. Amvrosiadis, A. A. Hwang, and B. Schroeder, "Temperature management in data centers: Why some (might) like it hot," *Sigmetrics '12*, no. TECHNICAL REPORT CSRG-615, pp. 163–174, 2012.

[13] V. A. Tsachouridis, P. Sobonski, H. Wiese, D. Mehta, K. Kouramas, and M. Cychowski, "Optimal Thermal Regulation of a Real Data Centre," IFAC-Pap., vol. 50, no. 1, pp. 4893–4898, Jul. 2017.

[14] K. Cho, H. Chang, Y. Jung, and Y. Yoon, "Economic analysis of data center cooling strategies," Sustain. Cities Soc., vol. 31, pp. 234–243, May 2017.

[15] H. Cheung, S. Wang, C. Zhuang, and J. Gu, "A simplified power consumption model of information technology (IT) equipment in data centers for energy system real-time dynamic simulation," Appl. Energy, vol. 222, pp. 329–342, Jul. 2018.

[16] E. Samadiani and Y. Joshi, "Proper Orthogonal Decomposition for Reduced Order Thermal Modeling of Air Cooled Data Centers," *J. Heat Transfer*, vol. 132, no. 7, p. 071402, 2010.

[17] E. Samadiani and Y. Joshi, "Reduced order thermal modeling of data centers via proper orthogonal decomposition: a review," *Int. J. Numer. Methods Heat Fluid Flow*, vol. 20, no. 5, pp. 529–550, 2010.

[18] R. Ghosh and Y. Joshi, "Error estimation in POD-based dynamic reduced-order thermal modeling of data centers," Int. J. Heat Mass Transf., vol. 57, no. 2, pp. 698–707, Feb. 2013.

[19] L. Phan and C.-X. Lin, "Reduced order modeling of a data center model with multi-Parameters," *Energy Build.*, vol. 136, pp. 86–99, 2017.

[20] M. Zapater, J. L. Risco-Martín, P. Arroba, J. L. Ayala, J. M. Moya, and R. Hermida, "Runtime data center temperature prediction using Grammatical Evolution techniques," Appl. Soft Comput., vol. 49, pp. 94–107, Dec. 2016.

[21] G. Varsamopoulos and M. Jonas, "Using transient thermal models to predict cyberphysical phenomena in data centers", *Informatics Syst.*, vol. 3, pp. 132–147, 2013.

[22] L. Wang, G. von Laszewski, F. Huang, J. Dayal, T. Frulani, and G. Fox, "Task scheduling with ANN-based temperature prediction in a data center: a simulation-based study," Eng. Comput., vol. 27, no. 4, pp. 381–391, Oct. 2011.

[23] U. Dvhg, R. I. Dqg, O. R. Z. Lq, J. Athavale, Y. Joshi, and M. Yoda, "Artificial Neural Network Based Prediction of Temperature and Flow Profile in Data Centers," 2018 17th IEEE Intersoc. Conf. Therm. Thermomechanical Phenom. Electron. Syst., pp. 871–880, 2020.

[24] V. A. Tsachouridis and T. Scherer, "Data centre adaptive numerical temperature models," vol. 40, no. 6, pp. 1911–1926, 2018.

[25] Z. Song, B. T. Murray, and B. Sammakia, "A compact thermal model for data center analysis using the zonal method," *Numer. Heat Transf. Part A Appl.*, vol. 64, no. 5, pp. 361–377, 2013.

[26] H. S. Erden, H. E. Khalifa, and R. R. Schmidt, “A hybrid lumped capacitance-CFD model for the simulation of data center transients,” *HVAC R Res.*, vol. 20, no. 6, pp. 688–702, 2014.
[27] Q. Tang, T. Mukherjee, S. K. S. Gupta, and P. Cayton, “Sensor-Based Fast Thermal Evaluation Model for Energy Efficient High-Performance Datacenters,” in 2006 Fourth International Conference on Intelligent Sensing and Information Processing, 2006, pp. 203–208.
[28] R. Sharma, C. Bash, C. Patel, R. J. Friedrich, and J. S. Chase, “Balance of Power: Dynamic Thermal Management for Internet Data Centers,” IEEE Internet Comput., vol. 9, pp. 42–49, Jan. 2005.
[29] J. W. Axley, “Surface-drag flow relations for zonal modeling,” Build. Environ., vol. 36, no. 7, pp. 843–850, Aug. 2001.
[30] F. Haghighat, Y. Li, and A. C. Megri, “Development and validation of a zonal model — POMA,” Build. Environ., vol. 36, no. 9, pp. 1039–1047, Nov. 2001.
[31] J. Gao, J. Zhao, X. Li, and F. Gao, “A Zonal Model for Large Enclosures with Combined Stratification Cooling and Natural Ventilation: Part 1—Model Generation and its Procedure,” J. Sol. Energy Eng., vol. 128, no. 3, pp. 367–375, Aug. 2006.
[32] E. Wurtz, J. M. Nataf, and F. Winkelmann, “Two- and three-dimensional natural and mixed convection simulation using modular zonal models in buildings,” *Int. J. Heat Mass Transf.*, vol. 42, no. 5, pp. 923–940, 1999.
[33] J. Gao, J. Zhao, X. Li, and F. Gao, “Evaluation of a Zonal Model for Large Enclosures Using Computational Fluid Dynamics,” J. Asian Archit. Build. Eng., vol. 6, no. 2, pp. 379–385, Nov. 2007.
[34] H. Moazamigoodarzi, S. Pal, S. Ghosh, and I. K. Puri, “Real-time temperature predictions in IT server enclosures,” *Int. J. Heat Mass Transf.*, vol. 127, pp. 890–900, 2018.
[35] F. M. White, *Fluid Mechanics*, 7th ed. New York: McGraw-Hill, 2009.
[36] Z. M. Pardey, D. W. Demetriou, J. W. Vangilder, H. E. Khalifa, and R. R. Schmidt, “Proposal for Standard Compact Server Model for Transient Data Center Simulations,” *Ashrae*, vol. 121, no. January, pp. 413–422, 2015.
[37] M. Iyengar and R. Schmidt, “Analytical Modeling for Thermodynamic Characterization of Data Center Cooling Systems,” *J. Electron. Packag.*, vol. 131, no. 2, p. 021009, 2009.
[38] Product Data Sheet, *Trane*, Air-Cooled Liquid Chillers 10 to 60 Tons, CG-PRC007-EN, April 2004.
[39] Product Data Sheet, *RITTAL*, TopTherm LCP Rack/Inline CW, Model Number: 3311.130/3311.530, 2015.
[40] Product Data Sheet, *ebm-papst* , EC centrifugal fan, Model Number: R3G250-RO40-A9, 2012.
[41] R. K. Shah and D. P. Sekulic, Fundamentals of Heat Exchanger Design. John Wiley & Sons, 2003.
[42] Y. Fulpagare, Y. Joshi, and A. Bhargav, “Rack level forecasting model of data center,” in 2017 16th IEEE Intersociety Conference on Thermal and Thermomechanical Phenomena in Electronic Systems (ITherm), 2017, pp. 824–829.
[43] C. M. Liang, L. Li, J. Liu, S. Nath, A. Terzis, and C. Faloutsos, “ThermoCast: A Cyber-Physical Forecasting Model for Data Centers Categories and Subject Descriptors,” *7th ACM SIGKDD Int. Conf. Knowl. Discov. Data Min.*, pp. 1370–1378, 2011.
[44] J.Athavale, M.Yoda, and Y. Joshi, “Comparison of data driven modeling approaches for temperature prediction in data centers,” *Int. J. Heat Mass Transf.*, vol. 135, pp. 1039–1052, 2019.